Colloid Polym Sci (2015) 293:3459–3469
DOI 10.1007/s00396-015-3717-2

ORIGINAL CONTRIBUTION

Composite of acicular rod-like ZnO nanoparticles and semiconducting polypyrrole photoactive under visible light irradiation for methylene blue dye photodegradation

Víctor M. Ovando-Medina[1] · Raúl G. López[2] · Blanca E. Castillo-Reyes[3] · Pedro A. Alonso-Dávila[3] · Hugo Martínez-Gutiérrez[4] · Omar González-Ortega[3] · Lorena Farías-Cepeda[5]

Received: 5 March 2015 / Revised: 1 July 2015 / Accepted: 19 July 2015 / Published online: 1 August 2015

Abstract Nanoparticles of zinc oxide (ZnO) with acicular rod-like morphology were synthesized using a bicontinuous microemulsion and coated with polypyrrole (PPy), by polymerization in the presence of dioctyl sodium sulfosuccinate (AOT) surfactant with ammonium persulfate as oxidizing agent to obtain nanocomposites of ZnO/PPy. The resulting material was characterized by FTIR, Raman spectroscopy, and scanning electron microscopy. The synthesized nanocomposite consisted of ZnO nanoparticles immersed in a polypyrrole matrix with a conductivity of 6.4×10^{-6} S/cm. The synthesized nanocomposite was tested in the photodegradation of methylene blue (MB) dye under visible light irradiation resulting in photodegradation efficiency of 95.2 % after 60 min of irradiation using 3.6 g/L of nanocomposite in an aqueous solution of MB at 20 mg/L. Pseudo first-order kinetics were used to describe the photodegradation reactions.

✉ Víctor M. Ovando-Medina
ovandomedina@yahoo.com.mx

[1] Ingeniería Química, Coordinación Académica Región Altiplano (COARA), Universidad Autónoma de San Luis Potosí, Carretera a Cedral KM 5+600, San José de las Trojes, Matehuala, SLP 78700, Mexico

[2] Centro de Investigación en Química Aplicada, Boulevard Enrique Reyna Hermosillo No. 140, 25253 Saltillo, Coah, Mexico

[3] Facultad de Ciencias Químicas, Universidad Autónoma de San Luis Potosí. Av. Dr. Manuel Nava No.6, Zona Universitaria, San Luis Potosí, SLP 78240, Mexico

[4] Centro de Nanociencias y micro y nanotecnologías, Instituto Politécnico Nacional, Luis Enrique Erro S/N, DF 07738, Mexico

[5] Departamento de Ingeniería Química, Facultad de Ciencias Químicas, Universidad Autónoma de Coahuila, Blvd. V. Carranza e Ing. José Cárdenas V. S/N, Saltillo, Coahuila 25280, Mexico

Keywords ZnO/polypyrrole · Nanocomposites · Photocatalyst · Visible light

Introduction

Zinc oxide (ZnO) has been considered a promising low-cost photocatalyst with physical and chemical stability, high oxidative capacity, and availability [1]; however, due to its bad gap (*ca*. 3.25 eV [2]) it is photoactive only under UV light irradiation ($265<\lambda<370$ nm) which is dangerous and expensive [3]. It has been demonstrated that ZnO particles with morphology in the nanometric scale show improved performance due to its large surface area, short carrier diffusion length, and low reflectivity [4].

Several works have reported the synthesis and characterization of ZnO/PPy composites for a variety of uses. For example, Barkade et al. [5] reported the ultrasound-assisted syntheses of PPy/ZnO latexes by miniemulsion polymerization for liquefied petroleum gas sensing. These authors obtained spherical ZnO nanoparticles with size between 80 and 100 nm, which were well coated with PPy; the final diameter of the ZnO/PPy nanoparticles was in the range from 160 to 190 nm. Oaki et al. [6] prepared ZnO nanorods by deposition onto indium tin oxide (ITO) through an aqueous solution process; afterwards, a layer of PPy was deposited to obtain nanostructures with enhanced performance as photoswitches and photodetectors. de Melo et al. [7] prepared fluorescent fibers of polyvinyl alcohol/PPy-ZnO by an electrospinning method. They observed that when the fluorescence emission at 390 nm of ZnO nanoparticles is quenched, the fibers exhibited a visible emission at 526 nm with a well-defined green coloration.

To shift the ZnO photoactivity toward the visible light region, Wang et al. [8] synthesized nanorod arrays (with

diameter of 150–170 nm and 1.5 μm in length) of ZnO onto ITO substrate by electro-deposition followed by pyrrole polymerization using ferric chloride ($FeCl_3$) as oxidizing agent. As a result, they obtained sensitized composites of ZnO/PPy which were used as efficient electrodes in a photoelectrochemical water-splitting process. Composites of ZnO with semiconducting polyaniline have been developed as photocatalysts. Lin and Wu [9] prepared well-aligned ZnO nanotubes, by a hydrothermal process, coated with polyaniline (PANI) and used the resulting composite for the photodegradation of Rhodamine B under ultraviolet and visible light irradiation. They observed that the photocatalytic process followed first-order kinetics. Olad and Nosrati [10] prepared PANI/ZnO nanocomposite with core/shell morphology by in situ polymerization. They obtained spherical particles of 50 nm and used them for methylene blue photodegradation, observing high efficiency when visible light irradiation was used. More recently, Khatamian et al. [11] synthesized polythiophene (PT) onto ZnO to obtain PT/ZnO nanocomposite with different PT loading by in situ chemical oxidative polymerization, obtaining particles of 30 nm. These materials were efficient in the photodegradation of methyl orange under visible light irradiation.

In this work, ZnO/PPy nanocomposites were synthesized polymerizing pyrrole monomer by chemical oxidation onto ZnO nanoparticles of acicular rod-like morphology, previously obtained by precipitation from a bicontinuous microemulsion with high yield, and characterized by chemical, electrochemical, and electron microscopy procedures. The nanocomposite was tested as a photocatalyst in the degradation of methylene blue under visible light irradiation. To the best of our knowledge, this is the first time this nanocomposite with the aforementioned morphology is used in photodegradation of a dye in aqueous solutions using visible light irradiation.

Experimental

Materials

Pyrrole monomer (Py; >98 %), ammonium persulfate (APS; >98 %), dioctyl sodium sulfosuccinate (AOT; >96 %), $Zn(NO_3)_2 \cdot 6H_2O$ (99 %), sodium dodecyl sulfate (SDS) (>98.5 %), toluene (>99.8 %), and NaOH (98.9 %) were acquired from Sigma-Aldrich and used as received. Distilled grade water was used in all the experiments.

Preparation of ZnO/PPy nanocomposite

Preparation of ZnO/PPy nanocomposite is depicted in Fig. 1. First, ZnO nanoparticles were prepared by a precipitation method in a bicontinuous microemulsion system following the methodology reported elsewhere [12] and briefly described. A bicontinuous microemulsion composed of 40.5 wt.% surfactants (AOT/SDS 2/1 wt./wt.), 32.5 wt.% 0.7 M zinc nitrate aqueous solution, and 27 wt.% toluene was prepared. A 250-mL jacketed glass reactor (equipped with a reflux condenser and two inlets) was loaded with 100 g of microemulsion, raising the temperature to 70 °C under magnetic stirring. Afterwards, an aqueous NaOH solution (41.6 wt.%) was fed using a calibrated dosing pump (KdScientific, KDS-200). The dosing time of this solution was 15 min. The reaction proceeded for 30 min and acetone was added to precipitate the ZnO nanoparticles. Finally, the precipitate was washed several times with water-acetone mixture (80/20, wt./wt.) and dried at 70 °C to obtain purified ZnO nanoparticles (white dust, ≈90 % of yield).

Pyrrole polymerization onto ZnO nanoparticles was performed as follows: 30 g of water was mixed with 0.8 g of SDS in a 60-mL vial. Subsequently, 250 mg of ZnO nanoparticles was added and ultrasonicated (Cole-Parmer Instruments, CPX 130) for 10 min, 0.4 g of pyrrole was added and allowed to homogenize under magnetic stirring for 2 h. Then APS was dissolved in 10 mL of water (0.6 M) and added to the reaction mixture to start pyrrole polymerization. The reaction proceeded under magnetic stirring for 1 h. The reaction mixture was poured into an excess of methanol to precipitate the ZnO/PPy nanocomposite (black dust). The samples were decanted and dried at 60 °C in an oven for 24 h. Pyrrole conversions were determined gravimetrically by repeating the polymerizations, drying the total reaction mixture and subtracting the known weights of surfactant, APS, and ZnO from the total weight of dried samples.

Characterization

The resulting dried materials were analyzed by FTIR spectroscopy (Agilent, Cary 630) and Raman spectroscopy (B&W TEK INC.). SEM analysis was completed (JEOL high-resolution scanning electron microscope, JSM 7800F in STEM mode at 30 kV of beam acceleration) dispersing samples (1:100) in distilled water. A drop of the dispersed sample was poured onto a copper grid coated with Formvar™ resin and carbon film, afterwards it was allowed to dry overnight at room temperature. ZnO/PPy composite was analyzed by HR-TEM (JEOL, JEM ARM 200F) at 200 kV. Elemental analysis was performed by Energy Dispersive X-Ray Spectroscopy (EDS) using a detector coupled to the SEM. ZnO content of composite was determined by thermogravimetric analysis on a SDT Q600 (TA Instrument) between 25 and 800 °C, at a heating rate of 10 °C/min.

The electrical conductivities of samples were determined by the four-probe method (SP4 probe head Lucas/Signatone with 0.04 in. of spacing between tips) coupled to a Keithley instrument (2400 SourceMeter), the purified samples were

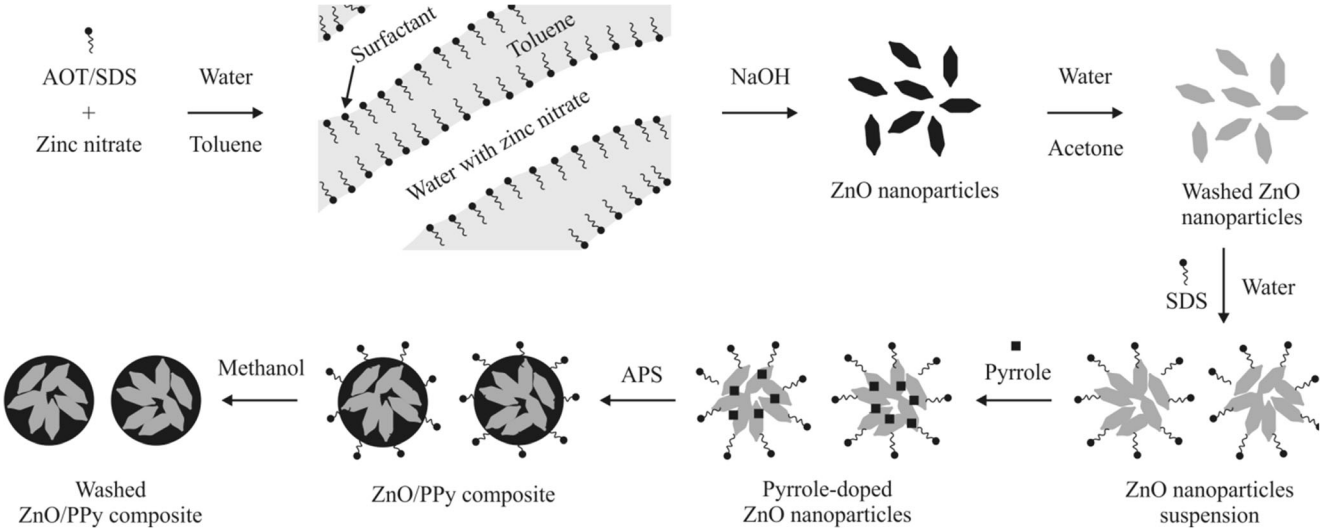

Fig. 1 Experimental procedure to obtain the ZnO/PPy composite

pressed in the shape of disks (1 cm of diameter×3 mm of thickness) using a weight of 2 t. The cyclic voltammetry measurements were performed in a glass cell using a potentiostat/galvanostat GAMRY (G-300). Platinum disk, platinum wire, and Ag/AgCl electrodes as the working, counter, and reference electrodes were used, respectively. Voltammetry scans were carried out at a scanning rate of 150 mV/s, dispersing 0.2 g of sample in 100 mL of 0.1 M KCl aqueous solution at room temperature in the potential range from +0.70 to +2.0 V for pure ZnO, and −0.6 to −0.1 V for the ZnO/PPy composite.

The composite was also analyzed using UV/Vis spectroscopy (Genesys 10, Thermo-Spectronic) as follows: 0.2 g of composite was dispersed in 5 mL of distilled water and ultrasonicated. Then 3 mL of dispersion was poured into a quartz cuvette and analyzed in the wavelength range from 250 to 1050 nm.

Photoactivity of synthesized materials

The synthesized ZnO/PPy nanocomposite was tested in methylene blue (MB) dye photodegradation in aqueous solutions. In Fig. 2, the experimental arrangement used is shown. The reactor consisted of a glass vessel with two quartz bulbs, the first for water recirculation at constant temperature (20 °C) and the second to insert the visible light source. 136, 241, and 542 mg of ZnO/PPy nanocomposite (0.90, 1.6, and 3.6 mg/L, respectively) were used in MB photodegradation experiments. For comparison purposes, pure ZnO (241 mg) was used in MB photodegradation as catalyst. The sample, either containing pure ZnO or ZnO/PPy nanocomposite was well dispersed in 150 mL of an aqueous solution of MB dye at 20 mg/L of initial concentration under magnetic stirring. In each case, as shown in Fig. 2, the tested solutions were exposed to a visible light source from a halogen lamp with tungsten filament (Philips LongLife EcoVision H7, 12 V, and 55 W). Samples of 0.5 mL were withdrawn at different times and centrifuged to determine UV/Vis spectra and absorbance (Genesys 10, Thermo-Spectronic) at a wavelength of 664 nm to calculate residual MB concentrations from a calibration curve. In addition, initial MB concentrations were varied from 20 to 100 mg/L when working with the ZnO/PPy composite with a fixed concentration of 1.6 mg/L. Experiments were carried out without the bubbling of air or oxygen.

To determine the removal of MB dye by physical adsorption, experiments similar to photodegradation using 542 mg of catalyst and 20 mg/L of MB dye initial concentration. Amount

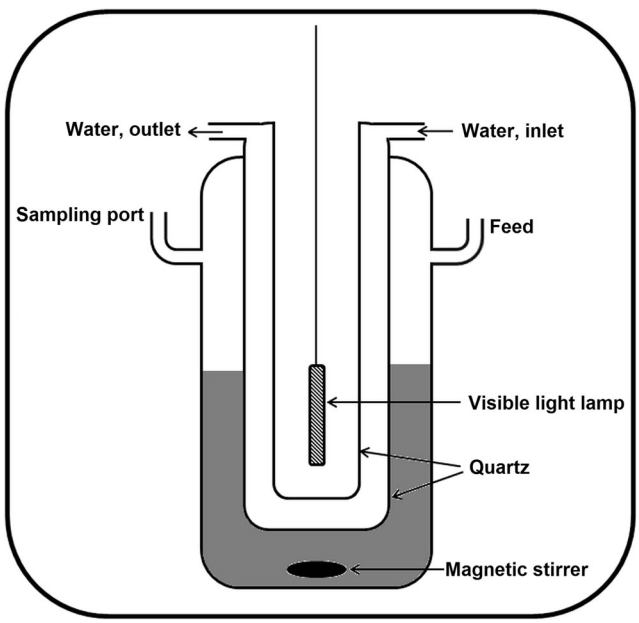

Fig. 2 Experimental arrangement used in MB photodegradations using ZnO/PPy composite under visible light irradiation

of MB dye removed by photolysis was studied exposing to the visible light irradiation a solution of MB dye of initial concentration of 20 mg/L without catalyst.

Results and discussion

The process to obtain the ZnO/PPy nanocomposite here described, implied first the synthesis of acicular rod-like ZnO nanoparticles by precipitation from a bicontinuous microemulsion. This is a very simple and easy way to achieve small particle sizes and high ZnO yields with the physical aspect of white dust. Afterwards, pyrrole monomer was polymerized by chemical oxidation onto purified ZnO nanoparticles, in this step, a small amount of surfactant was needed to stabilize the ZnO nanoparticles obtaining a PPy matrix in which the ZnO nanoparticles were immersed; as later demonstrated.

From a practical point of view, the ZnO/PPy nanocomposite can be removed easier than the pure ZnO nanoparticles from MB aqueous solutions, facilitating its recovery. The most interesting characteristic of the ZnO/PPy nanocomposite was its high photoactivity on the visible light range. From gravimetrical analysis, a pyrrole conversion of 50 % was determined; thus the final composite would have a weight ratio of ZnO to PPy of 55:45. However, from TGA analysis (shown in Appendix 1), the weight ratio of ZnO to PPy in the final composite was 43:58, which indicates that some of the ZnO particles might be loosen during the purification process.

Morphology of ZnO nanoparticles and ZnO/PPy composite

Figure 3a shows the SEM micrograph of ZnO nanoparticles synthesized in this work, whereas Fig. 3b shows the STEM image at higher magnification. As reported by Romo et al. [12], acicular rod-like morphology was observed in the ZnO nanoparticles, which demonstrates the reproducibility of their experiments. The size of these nanoparticles was in the range from 8 to 15 nm in diameter and between 20 and 35 nm in length. After pyrrole polymerization onto these ZnO nanoparticles, a composite consisting of a semiconducting PPy matrix in which ZnO nanoparticles were totally immersed can be observed (Fig. 4a).

Figure 4b shows the HR-TEM image of ZnO/PPy composite taken from a localized region within a single particle. Crystalline (circle) and amorphous (square) zones, which corresponds to ZnO and PPy, respectively, can be clearly seen. Using the *ImageJ 1.46a* software, it is found that the fringe spacing in the crystalline zone is about d=0.246 nm which further demonstrates the single-crystalline nature of the ZnO nanoparticles. The 0.246-nm length between the lattice fringes observed in the HR-TEM image agrees well with the spacing

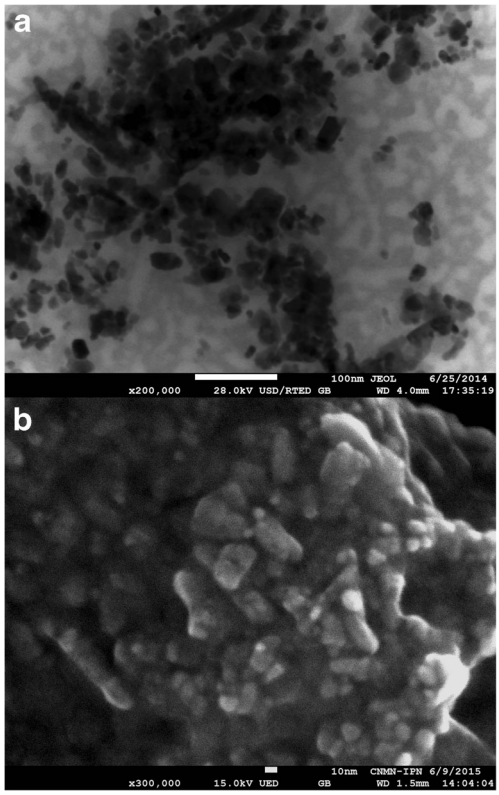

Fig. 3 SEM (**a**) and STEM (**b**) images of pure ZnO nanoparticles synthesized by precipitation in a bicontinuous microemulsion

of the (101) planes, which is in good agreement with the value reported in the literature (PDF card no. 036–1451).

Chemical composition of composite and conductivity

Figure 5 shows the Raman spectra of synthesized ZnO nanoparticles, pure PPy and the composite of ZnO/PPy. The main peaks of ZnO at 97, 330, 488, and 555 cm^{-1} can be observed. The signal at 330 cm^{-1} represents second-order Raman spectrum due to zone-boundary phonons of hexagonal ZnO, the peak at 488 cm^{-1} is ascribed to non-polar optical phonon E_2 of wurtzite ZnO, and the signal at 555 cm^{-1} can be attributed to A_1 (LO) mode of hexagonal ZnO [13]. Signal at 1043 cm^{-1} is not usually observed in ZnO, therefore this signal can be ascribed to residual surfactants used in the synthesis of ZnO as SDS and AOT (asymmetrical vibrations of C–C_{trans}). Signal at 97 cm^{-1} is due to E_2 low optical phonon. It can be seen from this figure that the curve corresponding to pure PPy presents the main signal characteristics of PPy of the reduced state at 1572 cm^{-1}, related to a mixed νC=C and inter-ring νC–C vibration, 1306, 1238, 1070 and at 920 cm^{-1}, assigned to a ring deformation mode (δ_{ring}) [13]. The peak located at 1572 cm^{-1} is considered as a reflection of effective conjugated length. The greater the red shift of this peak, the longer is the effective conjugated length of the conducting polymer.

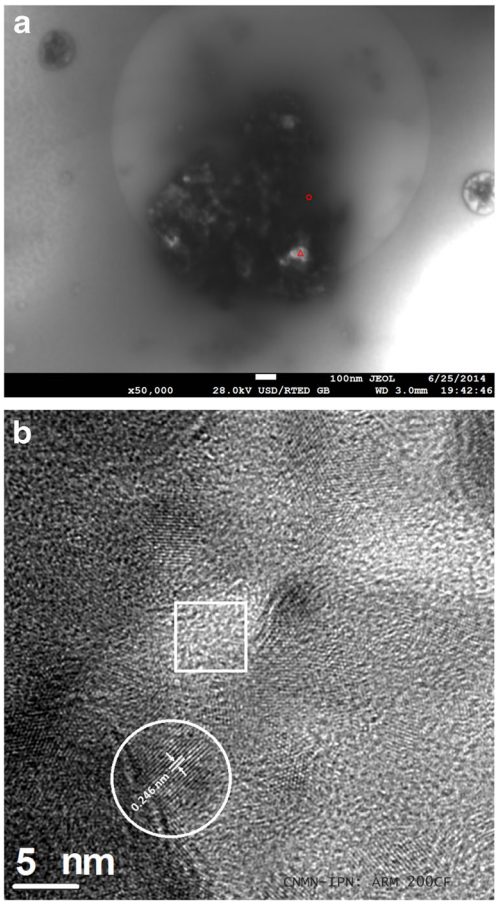

Fig. 4 SEM (**a**) and HR-TEM (**b**) images of ZnO/PPy composite. *Circle* and *square* in (**b**) show crystalline and amorphous zones, respectively

Combined and new signals of ZnO and PPy were observed in Fig. 5 indicating the interaction of ZnO and PPy in the composite.

Figure 6 shows the FTIR spectra of ZnO nanoparticles (a), ZnO/PPy composite (b), and pure PPy (c). It can be observed from curve (a) that the typical signal of ZnO interaction in stretching mode was near to 893 cm^{-1} [5, 14]. The presence of PPy can be observed in curves (b and c) where characteristic signals were present: the band at 1560 cm^{-1} and a weak band at 1470 cm^{-1} are assigned to stretching vibration of C=C and C–C in the pyrrole ring while the peak at 1075 can be ascribed to C–N stretching vibrations. The peak located at 1560 cm^{-1} is considered as a reflection of effective conjugated length. The greater the red shift of this peak, the longer the effective conjugated length of the conducting polymer [15–17]. The peak corresponding to ZnO in curve (b) is almost absent, which indicates that ZnO nanoparticles were well coated with PPy.

Figure 7 shows the elemental analysis obtained by EDS run at two zones of the SEM image (shown as triangular and circular areas in Fig. 4). It can be seen in Fig. 7 that the triangular area corresponds to a zone with a high content of ZnO whereas the circular area corresponds to organic material (PPy rich). With these results, it can be concluded that ZnO nanoparticles were well distributed into the PPy matrix. Additionally in both EDS spectra from Fig. 7, other elements are observed, such as S and Na, which indicates that some surfactant molecules and oxidizing agents remained even after composite purification.

In Fig. 8 the UV/Vis spectra of ZnO nanoparticles (a) and ZnO/PPy composite (b) are shown. The uncoated ZnO nanoparticles had a strong absorption in the UV region with spectral wavelength between 250 and 400 nm, which is similar to that reported by Wang et al. [8]. On the other hand, the ZnO/PPy composite showed absorption above the uncoated ZnO nanoparticles in the visible region with the absorption edge

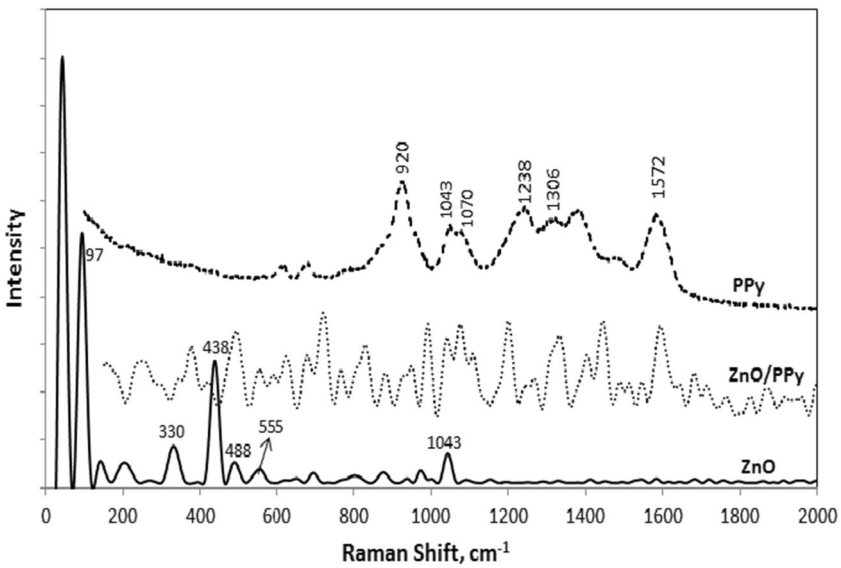

Fig. 5 Raman spectra of ZnO nanoparticles, PPy and ZnO/PPy composite

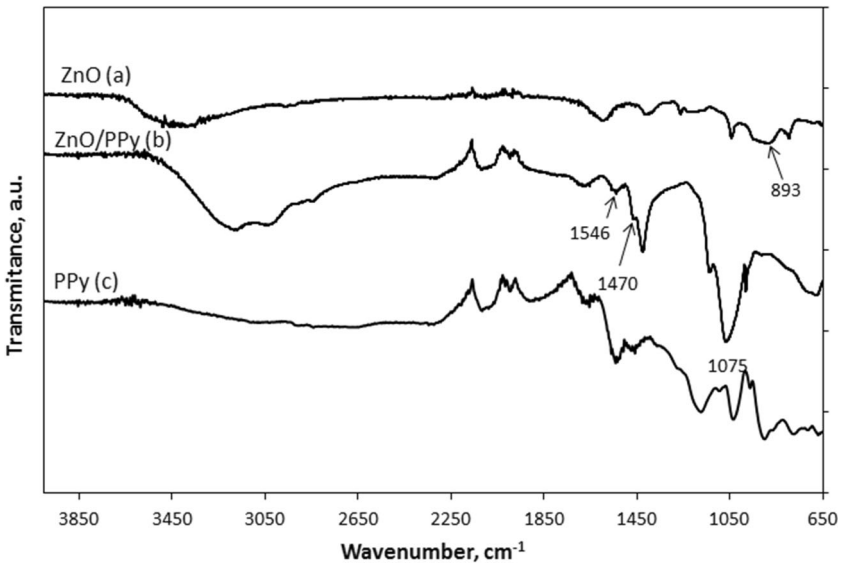

Fig. 6 FTIR spectra of ZnO nanoparticles, ZnO/PPy composite and pure PPy

shifted toward longer wavelength, this behavior can be ascribed mainly to the presence of semiconducting PPy.

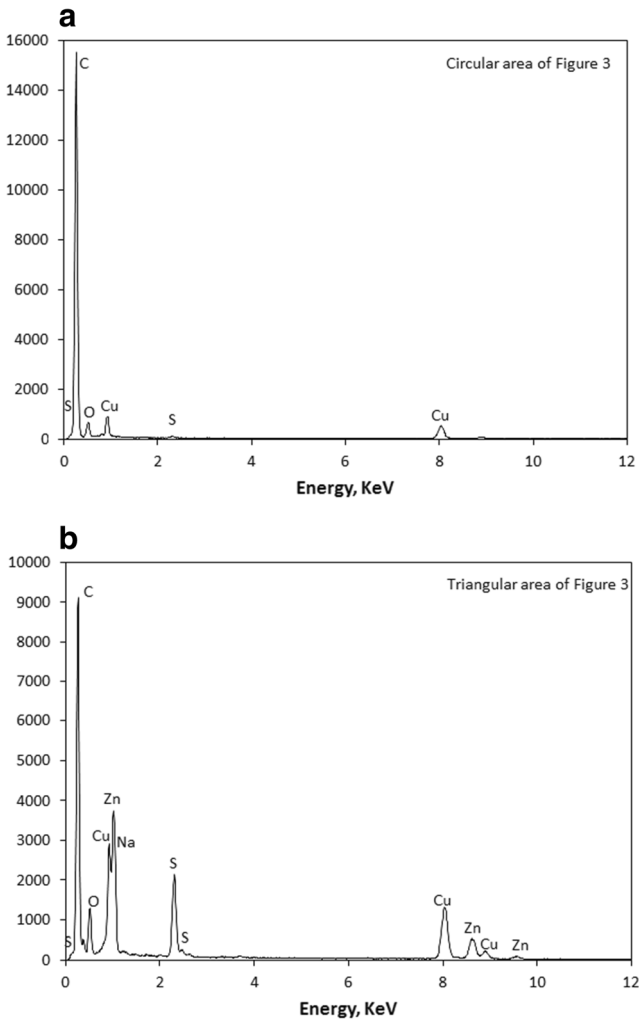

Fig. 7 EDS spectra of ZnO/PPy composite: **a** *Circular* and **b** *triangular* areas of Fig. 4, respectively

Two absorption bands with maxima at 460 and 960 nm were observed in the spectrum of the composite (Fig. 8). The first band is attributed to transitions of the valence band to the polaron state, which is directly related to the conductivity of the PPy chain (high degree of π-conjugation, i.e., π–π* interactions along the polymer chain). The second band is related to the bipolaron state. The bipolaron state is common when some dopant is present in the conducting polymer chain. In this work, the bipolaron state can be ascribed to the presence of surfactant molecules used throughout the synthesis, which act as dopants [17, 18]. The conductivity values for pure ZnO and ZnO/PPy were 7.9×10^{-10} S/cm and 6.4×10^{-6} S/cm, respectively; thus the presence of PPy increased not only photoactivity (Fig. 8) of the composite but its conductivity.

The electrochemical properties of ZnO nanoparticles and ZnO/PPy composite were studied by cyclic voltammetry. The voltammetry curves of synthesized materials are shown in Fig. 9. The ZnO nanoparticles showed negligible redox activity (inset in Fig. 9) compared to ZnO/PPy composite. The cathodic and anodic peaks of ZnO were +1.4 and +0.85 V, respectively. Here the characteristic redox behavior of PPy is clearly seen, with an oxidation peak (cathodic) around −0.24 V while the reduction peak (anodic) is near to −0.48 V vs. Ag/AgCl for the sample of ZnO/PPy composite. Typical values of potential corresponding to cathodic and anodic peaks for pure PPy are approximately +0.20 and −0.15 V vs. Ag/AgCl [19]. Thus, the presence of ZnO shifted the potentials of cathodic and anodic peaks of PPy to lower values. In other words, ZnO/PPy composite has lower oxidation potential.

Photocatalytic performance of composite

The photocatalytic performance of the ZnO/PPy composite was studied following the MB dye degradation in aqueous solutions

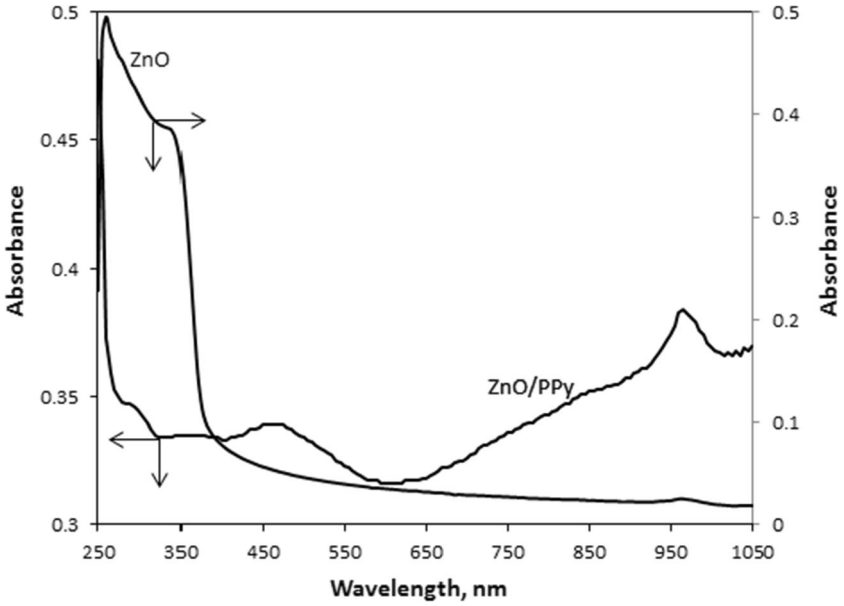

Fig. 8 UV/Vis spectra of ZnO nanoparticles and ZnO/PPy composite

under visible light irradiation. Figure 10 shows the ratio of residual to initial MB concentration (C/C_0) as a function of time using the ZnO/PPy composite (540 mg) for different MB initial concentrations. It can be observed that 93.3 % of degradation efficiency can be achieved after only 30 min of visible light exposition (for the smallest value of MB initial concentration). When the MB initial concentration was increased, maintaining constant the catalyst load fixed to 540 mg, lower degradation efficiencies were observed (71.8 and 55.9 % for 50 and 100 mg/L of MB initial concentration, respectively) after 30 min of irradiation. Furthermore, only 1 min was needed to achieve 68 % of degradation for 20 mg/L of initial MB concentration using 540 mg of ZnO/PPy composite.

As can be seen from Fig. 10, 8.8 % of MB was degraded by photolysis after 30 min of visible light irradiation, and only 9 % was achieved after 60 min of reaction. On the other hand, adsorption mechanism was considerable, giving 52 % of MB removal, it is important to observe that adsorption equilibrium is reached after 30 min. Therefore, photolysis, adsorption, and photodegradation mechanisms were present in our experiments.

Similar to the mechanism proposed by Wang et al. [20] for the photoactivity of TiO_2/PPy, when visible light collides with the composite ZnO/PPy, the electrons are promoted from the highest occupied molecular orbital (HOMO) to the lowest unoccupied molecular orbital (LUMO) of the semiconducting PPy,

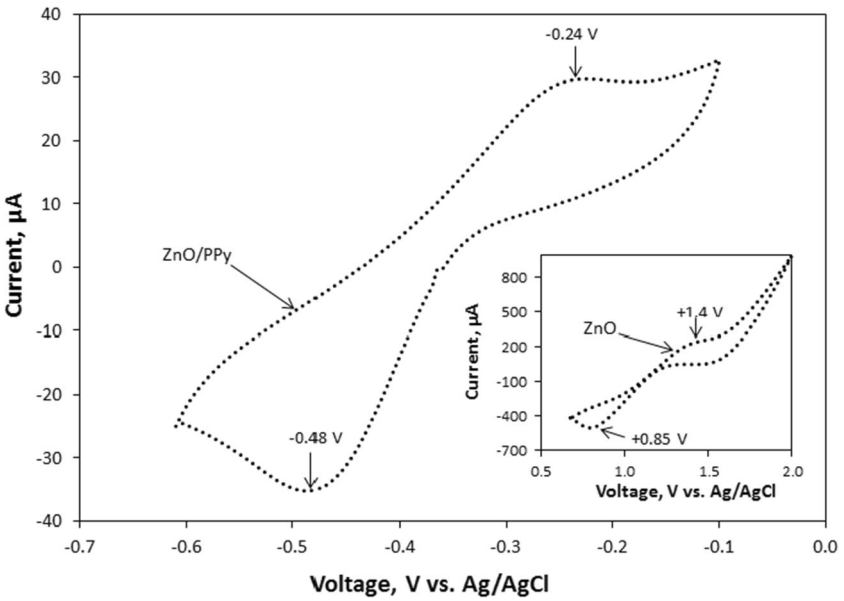

Fig. 9 Cyclic voltammetry curves of ZnO and ZnO/PPy

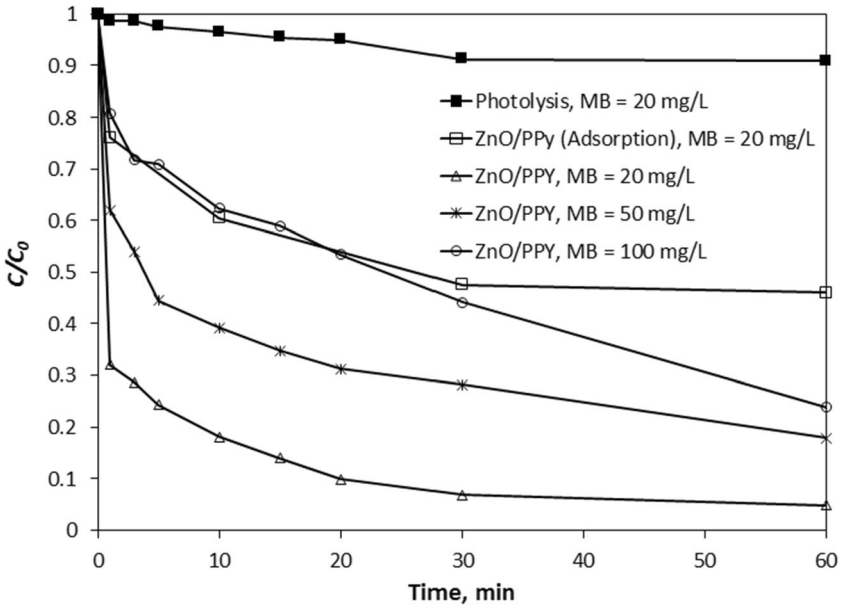

Fig. 10 Kinetics of MB dye photolysis, photodegradation under visible light irradiation and in the dark (adsorption) using ZnO/PPy composite for different MB initial concentrations. The catalyst load was 540 mg for each case, except for photolysis test where no catalyst was used

these electrons can be inserted to the conduction band (CB) of ZnO while holes will be left in the HOMO of PPy. The electrons in the valence band (VB) of ZnO can move to the HOMO of PPy to recombine with these holes and, at the same time, holes generate in the VB of ZnO. The photogenerated electrons are so active that they can react with O_2 (initially dissolved in water) to generate superoxide $\bullet O^-_2$, while holes can react with OH^- or water to generate •OH. These energetic species known as reactive oxygen species (ROS) can further react to form singlet oxygen $^1O_2$ [21]. On the other hand, adsorbed organic pollutants, such as dyes, can also absorb visible light, having a performance similar to the semiconducting PPy, injecting electrons to the conduction band of ZnO [22]. The overall reaction of dye photodegradation can be resumed as follows:

$$\text{Dye} + \text{ROS} \rightarrow \text{Degradated/mineralizated products} \quad (1)$$

When the reaction order for such photodegradation obeys the pseudo first-order kinetics, the following equation can be used:

$$-dC/dt = kC \quad (2)$$

where t represents the photodegradation time and k is the observed pseudo first-order rate constant. By integrating Eq. 2, the following expression is obtained:

$$-\ln(C/C_0) = kt \quad (3)$$

Thus, a plot of $-\ln(C/C_0)$ vs. time leads to a linear diagram which slope equals the observed pseudo first-order rate constant of photodegradation [23]. Figure 11 shows a plot of $-\ln(C/C_0)$ vs. time in which it can be observed that all photodegradations followed pseudo first-order kinetics, indicating that the photodegradation rate is directly proportional to MB concentration. The k value using 540 mg of catalyst and 20 mg/L of initial MB concentration for the ZnO/PPy composite was three times higher (k=0.055 min^{-1}) than that using 100 mg/L of initial MB concentration (k=0.0182 min^{-1}).

Figure 12 shows the effect of ZnO/PPy photocatalyst load on the photodegradation kinetics with a fixed initial MB concentration (20 mg/L) and the comparison with pure ZnO nanoparticles (241 mg). It can be observed that for pure ZnO nanoparticles, only 15.5 % of degradation efficiency was achieved after 30 min of visible light irradiation and 25.2 % after 60 min. This change in the residual MB concentration in the aqueous phase can be due to a combined process of adsorption–degradation. When the amount of MB physically adsorbed onto pure ZnO is enough to act as photosensitizer, photons of visible light irradiation can move electrons from the MB molecules and be transferred to the conduction band of ZnO, similar to PPy. However, the efficiency is not comparable to the ZnO/PPy composite (63.5 % of degradation efficiency after 30 min for the same conditions). Decreasing the amount of ZnO/PPy by 2.25 times (from 542 to 241 mg), and after 60 min of degradation, resulted in a decrease in degradation efficiency from 95.2 to 75.6 %; while reducing four times the amount of ZnO/PPy composite dropped the degradation efficiency to 46.2 %, thus the photocatalyst amount strongly affects the efficiency of MB degradation.

A pseudo first-order kinetics was also observed in these cases (Fig. 13), with k=0.0075 min^{-1} using 136 mg of ZnO/PPy load, k=0.0164 min^{-1} for 241 mg of ZnO/PPy load, and k=0.055 min^{-1} for 541 mg of ZnO/PPy load. The

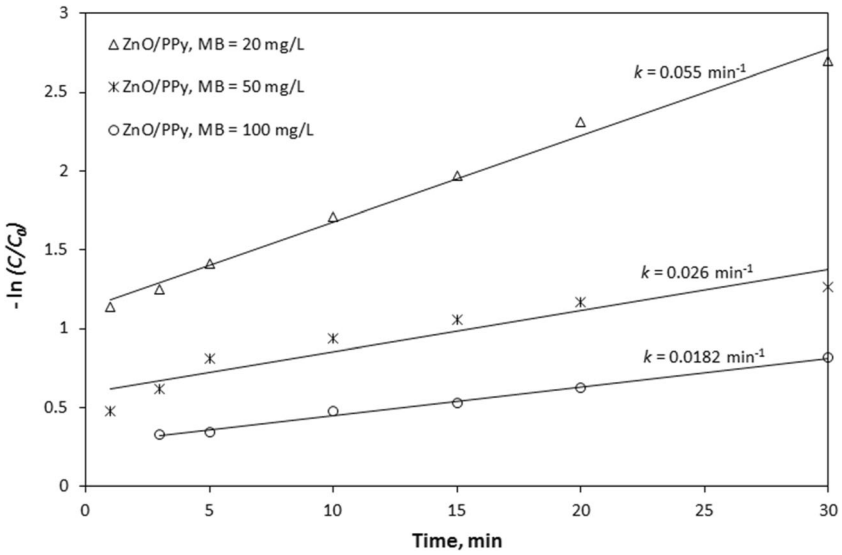

Fig. 11 $-\ln(C/C_0)$ as a function of time throughout MB dye photodegradation under visible light irradiation using ZnO/PPy composite for different MB initial concentrations. The catalyst load was 540 mg for each case

corresponding k value for pure ZnO nanoparticles was 0.0024 min^{-1}, which is very similar to that reported in the literature [1]. The k value using 241 mg of catalyst and 20 mg/L of MB initial concentration for the ZnO/PPy composite was approximately seven times higher (k= 0.0164 min^{-1}) than that corresponding to pure ZnO nanoparticles (k=0.0024 min^{-1}), showing the enhanced performance of the ZnO/PPy composite under the studied conditions.

The results of this work can be compared to those reported by Rajbongshi et al. [1] whom tested pristine ZnO nanoparticles, synthesized by precipitation using zinc acetate as precursor, and Ag-deposited ZnO nanoparticles in the photodegradation of MB dye under visible light irradiation (they did not report MB initial concentration nor photocatalyst load). Similar to our findings, they observed pseudo first-order kinetics in the photodegradation of MB, however only 15 % of photodegradation efficiency was observed for pristine ZnO and 50 % for the Ag/ZnO composite after 60 min of visible light irradiation. The corresponding k values were 0.0026 min^{-1} for pristine ZnO and 0.014 min^{-1} for Ag/ZnO composite, which is four times lower than our ZnO/PPy composite (using 540 mg of catalyst and 20 mg/L of initial MB concentration). On the other hand, Olad and Nosrati [10] used 1.5 g of PANI/ZnO composite and 50 mL of MB dye solution (10 mg/L), exposed to visible light irradiation, observing a degradation efficiency of 82 % after 60 min. Thus semiconducting PPy is more effective than PANI when combined with ZnO.

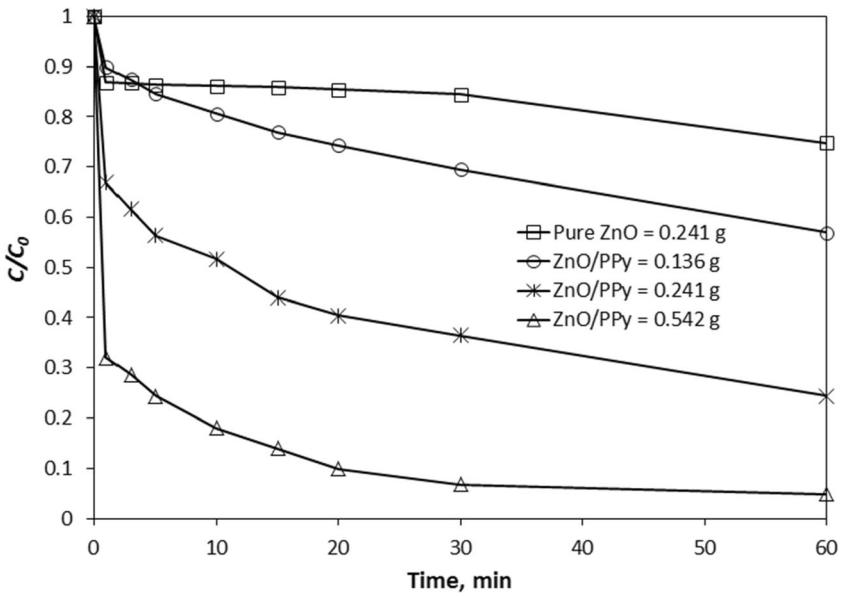

Fig. 12 MB dye photodegradation kinetics under visible light irradiation using pure ZnO nanoparticles and different ZnO/PPy composite loading

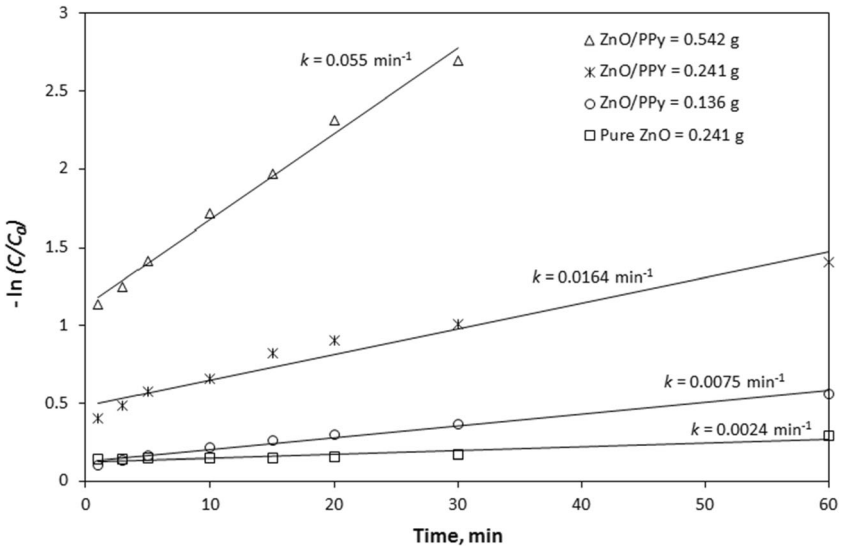

Fig. 13 $-\ln(C/C_0)$ as a function of time for MB dye photodegradation under visible light irradiation using different ZnO/PPy composite loading

Conclusions

ZnO nanoparticles were synthesized with high yield by precipitation from a bicontinuous microemulsion and coated with semiconducting PPy by chemical oxidation to obtain ZnO/PPy nanocomposite. It was observed that ZnO nanoparticles were totally immersed into a PPy matrix and showed photoactivity not only in the wavelength region of the UV light but also in the visible light region with increased conductivity. Photocatalytic performance of the nanocomposite was demonstrated in the MB dye degradation under visible light irradiation, showing efficiencies as high as 95.2 % after 60 min of reaction following a pseudo first-order mechanism.

Acknowledgements B.E. Castillo-Reyes acknowledges the scholarship from CONACYT (229857). V.M.O.M. wants to thank the Consejo Nacional de Ciencia y Tecnología—México by Grant # SEP-80843. V.M.O.M. thanks the hospitality of Dr. Farías-Cepeda at the sabbatical leave in Facultad de Ciencias Químicas, Universidad Autónoma de Coahuila.

Appendix 1

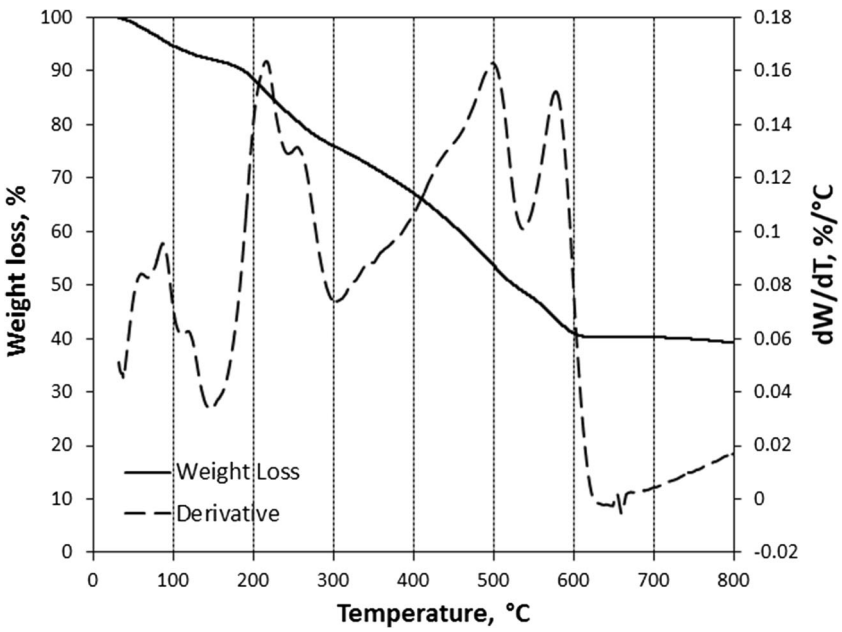

Fig. 14 TGA analysis of ZnO/PPy composite

References

1. Rajbongshi BM, Ramchiary A, Jha BM, Samdarshi SK (2014) Synthesis and characterization of plasmonic visible active Ag/ZnO photocatalyst. J Mater Sci Mater Electron 25:2969–2973. doi:10.1007/s10854-014-1968-1
2. Senadeera GKR, Kitamura T, Wada Y, Yanagida S (2006) Enhanced photoresponses of polypyrrole on surface modified TiO_2 with self-assembled monolayers. J Photochem Photobiol A 184:234–239. doi:10.1016/j.jphotochem.2006.04.033
3. Wu T, Lin T, Zhao J, Hidaka H, Serpone N (1999) TiO_2-assisted photodegradation of dyes. 9. Photooxidation of a squarylium cyanine dye in aqueous dispersions under visible light irradiation. Environ Sci Technol 33:1379–1387. doi:10.1021/es980923i
4. Zhong M, Li Y, Yamada I, Delaunay JJ (2012) ZnO–$ZnGa_2O_4$ core–shell nanowire array for stable photoelectrochemical water splitting. Nanoscale 4:1509–1514. doi:10.1039/C2NR11451H
5. Barkade SS, Pinjari DV, Singh AK, Gogate PR, Naik JB, Sonawane SH, Ashokkumar M, Pandit AB (2013) Ultrasound assisted miniemulsion polymerization for preparation of polypyrrole–zinc oxide (PPy/ZnO) functional latex for liquefied petroleum gas sensing. Ind Eng Chem Res 52:7704–7712. doi:10.1021/ie301698g
6. Oaki Y, Oki T, Imai K (2012) Enhanced photoconductive properties of a simple composite coaxial nanostructure of zinc oxide and polypyrrole. J Mater Chem 22:21195–21200. doi:10.1039/C2JM34525K
7. de Melo EF, Alves KGB, Junior SA, de Melo CP (2013) Synthesis of fluorescent PVA/polypyrrole-ZnO nanofibers. J Mater Sci 48:3652–3658. doi:10.1007/s10853-013-7159-2
8. Wang Z, Xiao P, Qiao L, Meng X, Zhang Y, Li X, Yang F (2013) Polypyrrole sensitized ZnO nanorod arrays for efficient photoelectrochemical splitting of water. Physica B Condens Matter 419:51–56. doi:10.1016/j.physb.2013.03.021
9. Lin L, Wu Q (2012) Well-aligned ZnO nanotube/polyaniline photocatalysts for enhanced photocatalytic performances. Polym Polym Compos 20:367–376
10. Olad A, Nosrati R (2012) Preparation, characterization, and photocatalytic activity of polyaniline/ZnO nanocomposite. Res Chem Intermed 38:323–336. doi:10.1007/s11164-011-0349-0
11. Khatamian M, Fazayeli M, Divband B (2014) Preparation, characterization and photocatalytic properties of polythiophene-sensitized zinc oxide hybrid nanocomposites. Mater Sci Semicond Process 26:540–547. doi:10.1016/j.mssp.2014.04.038
12. Romo LE, Saade H, Puente B, López ML, Betancourt R, López RG (2011) Precipitation of zinc oxide nanoparticles in bicontinuous microemulsions. J Nano Mat 2011:1–9. doi:10.1155/2011/145963
13. Reddy AJ, Kokila MK, Nagabhushana H, Rao JL, Shivakumara C, Nagabhushana BM, Chakradhar RPS (2011) Combustion synthesis, characterization and Raman studies of ZnO nanopowders. Spectrochim Acta A 81:53–58. doi:10.1016/j.saa.2011.05.043
14. Batool A, Kanwal F, Imran M, Jamil T, Siddiqi SA (2012) Synthesis of polypyrrole/zinc oxide composites and study of their structural, thermal and electrical properties. Synth Met 161:2753–2758. doi:10.1016/j.synthmet.2011.10.016
15. Liu Y, Chu Y, Yang L (2006) Adjusting the inner-structure of polypyrrole nanoparticles through microemulsion polymerization. Mater Chem Phys 98:304–308. doi:10.1016/j.matchemphys.2005.09.025
16. González-Iñiguez JC, Ovando-Medina VM, Jasso-Gastinel CF, González DA, Puig JE, Mendizábal E (2014) Synthesis of polypyrrole nanoparticles by batch and semicontinuous heterophase polymerizations. Colloid Polym Sci 292:1269–1275. doi:10.1007/s00396-014-3177-0
17. Ovando-Medina VM, Peralta RD, Mendizábal E, Martínez-Gutiérrez H, Lara-Ceniceros T, Ledezma-Rodríguez R (2011) Synthesis of polypyrrole nanoparticles by oil-in-water microemulsion polymerization with narrow size distribution. Colloid Polym Sci 289:759–765. doi:10.1007/s00396-011-2394-z
18. Choi J, Kim H, Haam S, Lee SY (2010) Effects of reaction sequence on the colloidal polypyrrole nanostructures and conductivity. J Disp Sci Tech 31:743–749. doi:10.1080/01932690903332954
19. Ovando-Medina VM, Diaz-Flores PE, Martínez-Gutiérrez H, Moreno-Ruiz LA, Antonio-Carmona ID, Hernández-Ordoñez M (2014) Composite of cellulosic agricultural waste coated with semiconducting polypyrrole as potential dye remover. Polym Compos 35:186–193. doi:10.1002/pc.22649
20. Wang D, Wang Y, Li X, Luo Q, An J, Yue J (2008) Sunlight photocatalytic activity of polypyrrole–TiO2 nanocomposites prepared by 'in situ' method. Catal Commun 9:1162–1166. doi:10.1016/j.catcom.2007.10.027
21. Liao Y, Brame J, Que W, Xiu Z, Xie H, Li Q, Fabian M, Alvarez PJ (2013) Photocatalytic generation of multiple ROS types using low-temperature crystallized anodic TiO2 nanotube arrays. J Hazard Mat 260:434–441. doi:10.1016/j.jhazmat.2013.05.047
22. Habib MA, Muslim M, Shahadat MT, Islam MN, Ismail IMI, Islam TSA, Mahmood AJ (2013) Photocatalytic decolorization of crystal violet in aqueous nano-ZnO suspension under visible light irradiation. J Nanostructure Chem 3:1–10. doi:10.1186/2193-8865-3-70
23. Montazerozohori M, Nasr-Esfahani M, Joohari S (2012) Photocatalytic degradation of an organic dye in some aqueous buffer solutions using nano titanium dioxide: a kinetic study. Environ Prot Eng 38:45–55. doi:10.5277/EPE120305